18th International Conference on Protection & Automation in Power Systems
Shahrood University of Technology
January 9, 2024 - January 10, 2024

2024 International Conference on Protection and Automation in Power Systems (IPAPS) | 979-8-3503-5038-8/24/$31.00 ©2024 IEEE | DOI: 10.1109/IEEECONF62358.2024.10453173

Design and Operation of Pulse Forming Network as Drive Circuit for Thomson Coil Actuator Used for High Voltage DC Circuit Breakers

Alireza Tabatabaei Malazi
Electrical Engineering Department
K. N. Toosi University of Technology
Tehran, Iran
a.tabatabaeimalazi@email.kntu.ac.ir

Seyed Hamid khalkhali
Electrical Engineering Department
K. N. Toosi University of Technology
Tehran, Iran
Hamidkhalhali@email.kntu.ac.ir

Mohsen Taghizadeh Kejani
Electrical Engineering Department
K. N. Toosi University of Technology
Tehran, Iran
mohsen.t.k@email.kntu.ac.ir

Ali A. Razi-Kazemi
Electrical Engineering Department
K. N. Toosi University of Technology
Tehran, Iran
razi.kazemi@kntu.ac.ir

Alireza Jafari
Electrical Engineering Department
K. N. Toosi University of Technology
Tehran, Iran
a.jafari@email.kntu.ac.ir

Alireza Rezapoor Barabady
Electrical Engineering Department
K. N. Toosi University of Technology
Tehran, Iran
a.rezapoorbarabady@email.kntu.ac.ir

***Abstract*— Thomson coil (TC) actuators are well studied for ultra-fast disconnectors (UFDs) where quick operation is desired, such as for hybrid high voltage direct current circuit breaker (HVDC CB) applications used in HVDC transmission line protection. In this paper, a novel driving circuit using pulse forming network (PFN) for TC has been proposed. Comprehensive multi-physic finite-element simulations of PFN-powered TC are carried out to assess the effect of various current pulses on the TC's electrical to mechanical energy conversion efficiency, in comparison to the efficiency achieved by using the typical capacitor bank discharge method. In this case, The TC can launch a 53-gram disk to a velocity of 9.4 m/s. The TC is powered by a 13.06 J PFN comprised of forty 196 V electrolytic capacitors; the selected PFN-powered TC obtained efficiency of 17%, which is substantially greater than conventional capacitor-powered TCs with 5 % efficiency.**

Keywords-Thomson coil; Ultra-fast disconnector; High voltage direct current; Circuit breaker; Pulse forming network; Efficiency

I. Introduction

Further development and extension of HVDC and FACTS are being driven by the rapid growth of power electronic and the urgent demand to integrate remote large-scale renewable energy sources into the pure HVDC or interconnected HVAC/HVDC systems [1-4]. For HVDC, there are several technical and economic superiority over conventional HVAC power transmission, such as being able to use both long underground and submarine cables or long overhead lines to transfer enormous amounts of power over great distances with low loss [5-8] and asynchronous connections between AC systems with various frequency ranges [9]. These superiorities necessitate the growth of multi-terminal HVDC systems [1]. Owing to the HVDC transmission lines low impedance, which causes fault current to rise rapidly, using an immediate detection and isolation of the faulted HVDC line is required for their protection [1, 10, 11]. Interruption is much more difficult for DC CB than it is for AC CB, because DC lacks zero-crossing, which aids fault isolation in the AC system [12]. DC CBs typically fall into three categories: solid-state circuit breakers (SSCBs), mechanical circuit breakers (MCBs), and hybrid circuit breakers (HCBs) [13-16]. The HCB configuration benefits from the solid-state breaker's fast operation speed and mechanical breakers carrying high load current with low on-state losses [17-19]. HCBs typically contain three branches: a normal operation branch that includes a load commutation swit-

18th International Conference on Protection & Automation in Power Systems
Shahrood University of Technology
January 9, 2024 - January 10, 2024

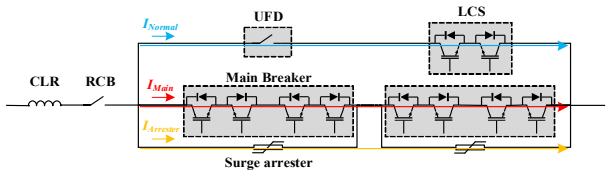

Figure 1. The structure of HCB.

ch (LCS) and an UFD; a main breaker branch comprised of number of power electronic switches (often IGBTs); and a surge arrester-based energy dissipation branch [13]. When the HCB is operating normally, current passes through its normal operation branch.; when the LCS receives a tripping signal, it will be immediately blocked and then the fault current will be commutated into the main breaker [2]. Simultaneously, the main breaker will be activated to provide a channel for the fault current. Once the fault current is entirely commutated into the main breaker, the UFD's contacts will begin to be separated under no current [13]. During this time, a current limiting reactor (CLR) is employed for reducing the rapidity of current rise (*di/dt*) [2]. Afterwards, the main breaker will be shut off, and the surge arresters dissipate the fault current [13]. Once the fault is removed, the residual current breaker (RCB) stops the flow of residual current and disconnects the damaged line from the HVDC network [20]. UFD is an ultra-fast mechanical switch [21] and it has a decisive impact on determining HCB's interruption time [17]. UFD requires a quick mechanical operation, typically accomplished by utilizing a high-speed actuation mechanism. Hydraulic, pneumatic, linear motors, solenoid, magnetic, or spring-type actuation mechanisms all require many milliseconds to open contacts, making them unsuitable for DC breaking, while electromagnetic actuation mechanisms such as TC can attain a sub-millisecond level of opening time [11]. For HCBs to operate quickly, an electromagnetic UFD model equipped with a TC actuator must be used for system-level researches (transient stability, protection) and warranting proper HCB operation. The optimization approach focuses on designing a PFN-feeding TC instead of a conventional capacitor bank, which must provide a high-value current pulse with an appropriate duration injected into the TC. To maximize the actuator's electrical-to-kinetic conversion efficiency, this investigation offers some design considerations for a fieldable PFN system. A Multiphysics FEM software called COMSOL has been used to simulate and validate the optimization process. The simulated UFD is intended to attain a minimum 10 mm open distance (equal to 30kv dielectric strength in air). Furthermore, it might be expanded to accommodate high-voltage applications.

II. TC Actuator Principle

The principle of a TC-based UFD's fast opening and closing operations will be described, and the crucial parts are described below:

A. Structure and Mechanism of TC Actuator

Referring to Fig. 2, the four major components of the TC-based UFD are: 1) interrupter; 2) TC operating mechanism; 3) energy storage and control unit; 4) damping and holding mechanism [22].

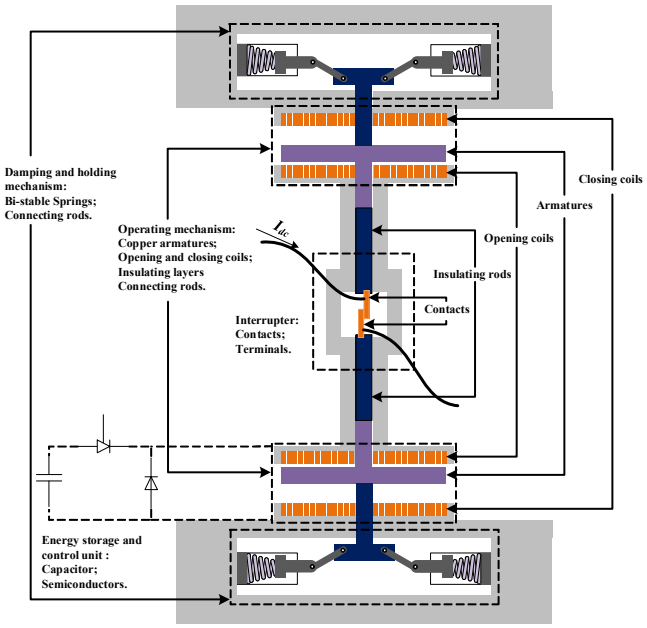

Figure 2. The main structure of UFD.

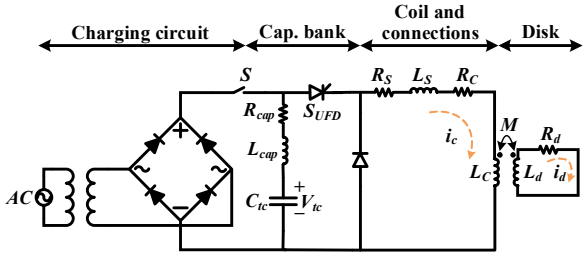

Figure 3. The equivalent circuit of the TC and driver.

Fig. 3 depicts the equivalent circuit for the TC and its driving circuit. When the capacitor bank C_{tc} reaches the voltage that equals V_{tc0}, switch S opens, separating the driving circuit from the charging circuit. When the UFD must open, the external signal from DC network protection will trigger the thyristor S_{UFD} of the opening coil. Activating S_{UFD} permits the capacitor bank that has been already charged to release its charge through the opening coil. By flowing the capacitor discharge current pulse through the opening coil i_c as seen in Fig. 5 [17], an alternating magnetic field is created. As a result, an induced eddy current i_a with reverse direction is generated on the disk [11] through mutual inductance M [17]. The induced current's direction and the resulting magnetic field creates a considerable force that causes the coil and the disk repel each other [11]. Because the coil is fixed tightly by its holder on an immovable structure, the disk together with the moving contact will be repulsed to travel downward and separate the contacts at a high speed. In this specific circuit, the diode restricts the rate at which the current decays once it has peaked. The closing process is carried out similarly by triggering another thyristor that allows the current flow through the closing coil. Afterwards, the disk travels toward the top, closing the contacts. Bi-stable springs with hold and latch mechanisms stop this movement. This spring's action absorbs a significant portion of mechanism's kinetic energy, dampening the motion until it comes to a stop [22].

18th International Conference on Protection & Automation in Power Systems
Shahrood University of Technology
January 9, 2024 - January 10, 2024

B. Design of the TC Actuator

Fig. 4 depicts the design variables of a TC, while TABLE I presents the parameters data concerning the TC and its driving circuit. The TC consists 13 turns of enameled rectangular cross-section conductors in the dimensions of 0.8×2.50 mm^2. The coil's inner and outer radius are 6 mm and 24.1 mm, respectively, which are embedded in a holder, and fixed with epoxy resin. A repulsive disk with the mentioned dimensions in TABLE I is placed with a 0.1 mm air gap in the proximity of the coil.

C. UFD's Electrodynamic Model

1) TC and Driver Electrical Circuit Modeling

The following are the formulas for the driving circuit and the single-turn circuit (1)-(2):

$$R_1 i_c + L_1 \frac{di_C}{dt} - \frac{d(Mi_d)}{dt} = V_{tc} \quad (1)$$

$$R_d i_d + L_d \frac{di_d}{dt} - \frac{d(Mi_c)}{dt} = 0 \quad (2)$$

$$R_1 = R_C + R_S + R_{Cap},\ L_1 = L_C + L_S + L_{Cap}$$

R_C, R_S, R_{Cap}, and R_d are the primary coil resistivity, stray resistivity of the connections, the capacitor resistivity, and disk resistivity, respectively, L_{Cap}, L_s, L_c, L_d, and M are the capacitor inductance, stray inductance, coil inductance, disk inductance, and mutual inductance, respectively [17]. The capacitor bank stores the following amount of electrical energy:

$$E_{Cap} = 0.5 C_{tc} {V_{tc}}^2 \quad (3)$$

2) Dynamic Mechanical Model

This system's electromagnetic energy (W_e) consists of the stored energy in the coil, the mutual inductance, and the disk that is written down:

$$W_e = \frac{1}{2} L_c i_c^2 + \frac{1}{2} L_d i_d^2 - M i_d i_c \quad (4)$$

Differentiating (4) gives the repulsive electromagnetic force between coil and disk [17]:

$$F_e = -\frac{\mathrm{d}w_e}{\mathrm{d}z} = \frac{\mathrm{d}M}{\mathrm{d}z} i_d i_c \quad (5)$$

The drive current, eddy current, and derivative of the mutual inductance between the drive coil and the disk all participate in electromagnetic force [23]. The average velocity is as follows:

$$\bar{V} = \frac{\Delta z}{\Delta t} \quad (6)$$

Where Δz is the travel distance, and Δt is the travel time. The disk kinetic energy is as follows:

$$E_{kinetic} = 0.5 m \bar{V}^2 \quad (7)$$

Where m is the disk mass, and $\bar{V}$ is the average disk velocity:

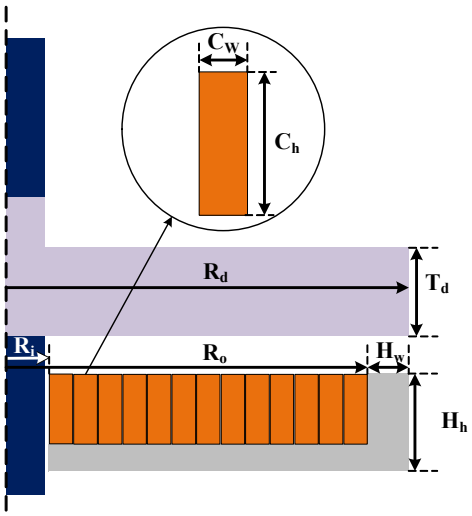

Figure 4. Simulated TC (coil, holder, and disk) dimensions.

TABLE I. TC AND DRIVER DESIGN PARAMETERS

parameter	Data	parameter	Data
Coil outer radius (R_o)	24.1 mm	Coil width (C_w)	0.8 mm
Coil inner radius (R_i)	6 mm	Coil height (C_h)	2.5 mm
Disk thickness (T_d)	10 mm	Holder height (H_h)	7 mm
Disk radius (R_d)	25 mm	Holder width (H_w)	4.5 mm
Disk mass	53 g	Capacitor (C_{tc})	2 mF
Disk material	Aluminum	voltage (V_{tc})	250 V
Holder material	Carbon steel	Coil turn	13

D. Opening Operation

Because the opening and closing operations are identical, this article exclusively examines the opening operation. Fig. 5 shows the results of opening operation obtained by discharging a 2 mF capacitor that has already been charged to 250 V. A current pulse of roughly 2.4 kA flows through the opening coil upon the capacitor bank discharge, which accelerates the disk in the first milliseconds. The disk then moves at an approximate average velocity of 10.4 m/s.

E. Computation of TC Electrical Characteristic

The inductance of a single-layer coil, which is measured in inches, can be calculated using equation (8).

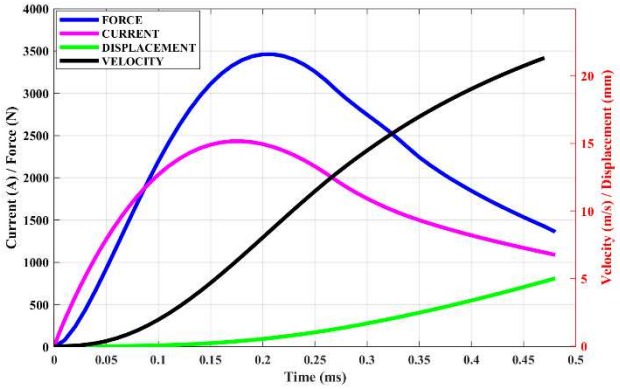

Figure 5. Simulation results for opening operation.

$$L_c = \frac{a^2 n^2}{8a+11c}\ (\mu H) \tag{8}$$

$$a = 0.5(R_o - R_i), c = (R_o - R_i)$$

Where n, a, and c represent the coil's turn number, average radius, and thickness, respectively [24]. The resonance frequency of the L-C current source will be roughly calculated as [25]:

$$f_{res} = \frac{1}{2\pi\sqrt{L_c C}}\ (\text{Hz}) \tag{9}$$

Where L_C is calculated according to (8), and C is equal to C_{tc}. The coil's inductive reactance and electrical resistance can be computed according to (10) and (11), respectively:

$$X_c = 2\pi f L_c \tag{10}$$

$$R_c = \rho \frac{L}{A} \tag{11}$$

Where ρ, L, and A are coil material resistivity, length, and cross-sectional area, respectively. According to (10) and (11), the coil impedance can be written as (12):

$$Z_c = R_c + jX_c \tag{12}$$

F. TC Issues

1) Efficiency

A TC actuator must actuate the disk as quickly as feasible for a predetermined time period while ensuring the efficiency (η) of energy transfer from storage to motion [11]. In a capacitively driven TC, a large current pulse flows through the coil, and a significant amount of inductive energy is lost in the air gap between coil and disk. The energy initially stored in the capacitor's electric field is divided into: (1) launch kinetic energy, (2) the joule heating of all subsystems, and (3) the remaining energy stored in the capacitor's and inductor's electric and magnetic fields. Approximately 5 % of the initial stored energy is typically transformed into kinetic energy [26-28], although recent researches claim efficiencies of up to 14% for loaded mechanisms [26]. Over the last decade, reported capacitive system efficiencies have not changed significantly. Low efficiency indicates a high need for energy storage. The efficiency of the capacitively driven TC is written as:

$$\eta_{Capacitor} = \frac{E_{kinetic}}{E_{Cap}} \times 100 \tag{13}$$

2) Maintenance and Reliability

Most TCs require many kilojoules of energy from capacitors, that are stored in millifarads of capacitance with kilovolts of voltage. Such high-voltage and high-capacitance capacitors require special care in their selection, implementation, and maintenance since they tend to gradually degrade over time [11], decreasing the capacitor's long-term reliability and lifetime. Furthermore, such a significant amount of energy might be highly hazardous for vulnerable loads in the case of fault occurrence [29]. These issues motivated research into designing, improving, and optimizing TC's driving circuit.

III. Pulse Forming Network (PFN)

PFNs are used to produce long, high-energy pulses, their limited stored energy and straightforward construction make them highly advantageous. Discrete capacitors and inductors combine to form the PFN, which is basically an open-ended transmission line. The transmission line theory explains the process of discharging the PFN capacitors and creating pulses using PFN as a lumped model of a transmission line [29]. Various types of PFNs have been documented in [30]. In this paper, a PFN structure as an option for limited stored energy in pulsed power use cases will be presented.

A. Input Data

The input data are the desired pulse width (T_P), rise time (T_r), current amplitude, number of sections (n), and load magnitude (see Fig. 6) [31].

B. Structure

Fig. 7 depicts a schematic representation of the PFN power supply [29]. The capacitance and inductance values of PFN sections (see Fig. 7) are calculated using Guillemin's theory and the input data [31]. In the simplest type, the transmission line is simulated using equal L-C ladders. The characteristic impedance (Z_0) and pulse width for this PFN with n equal sections are expressed as [29]:

$$T_P = 2n\sqrt{LC} \tag{14}$$

$$Z_0 = \sqrt[2]{\frac{L}{C}} \tag{15}$$

Each cell's inductance and capacitance are represented by the letters L and C. It is possible to estimate the matched load ($R_L = Z_0$) pulse's rise time as [29]:

$$T_r = 0.8\sqrt{LC} \tag{16}$$

The PFN's stored energy is as follows [29].

$$E_{PFN} = 0.5ncV^2 \tag{17}$$

Where n is the sections number, C is each section's capacitance, and V is the charging voltage.

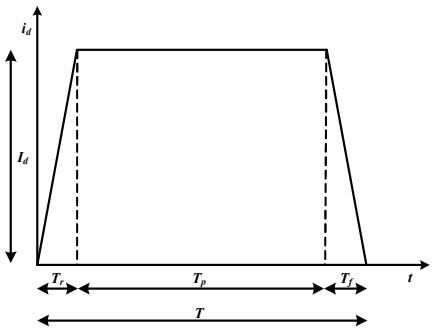

Figure 6. Required trapezoidal current pulse.

18th International Conference on Protection & Automation in Power Systems
Shahrood University of Technology
January 9, 2024 - January 10, 2024

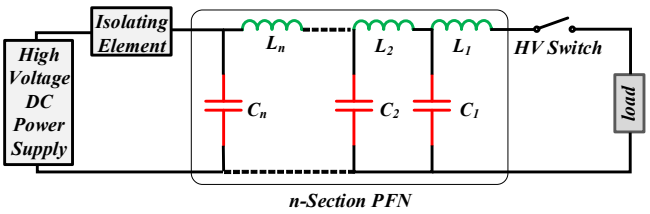

Figure 7. Block diagram of a PFN power supply.

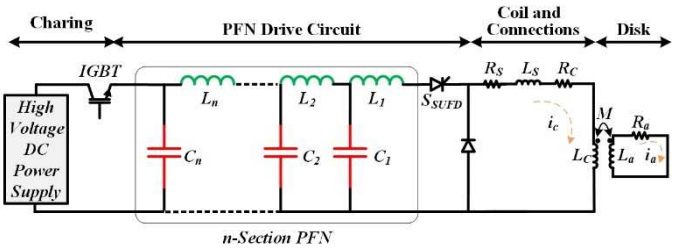

Figure 8. Equivalent circuit diagram of the proposed PFN-powered TC actuator.

IV. PFN as Drive Circuit for TC

Most implementations of TC-based UFD, employ drive circuits that inject a current pulse into the coil by discharging a capacitor bank, as shown in Fig. 3. This paper presents investigations on using PFN as a drive circuit instead of a conventional capacitor bank, as shown in Fig. 8.

A. Design Procedure

This research develops an analytical approach that expedites the optimization process, assuming that the TC has a linear equivalent resistance (R_L) equal to its impedance (Z_C); the nonlinearity of TC is ignored when determining its impedance. Therefore, the impedance (Z_0) is assumed constant in the calculation of the capacitance and inductance of PFN cells using equations (14)-(16) for this laboratory-scale simulated TC. One requirement for the PFN-powered TC is that its output current profile should be similar to its capacitor-powered TC. The charging voltage of PFN cells is determined by taking into account the resistive-inductive TC load characteristics and the desired current pulse characteristics. The initial charging voltage of PFN is modified after running the computer simulation several times until the desired current pulse profile is achieved. The PFN characteristic impedance (Z_0) is matched to the load impedance (Z_C) to achieve maximum energy transfer in the main pulse.

B. Efficiency

The PFN-powered TC has demonstrated efficiencies considerably above the typical capacitor-powered 5 % efficiency. As a result, energy storage and prime power requirements would be decreased which are described below. The efficiency of the PFN-powered TC actuator is written as:

$$\eta_{PFN} = \frac{E_{kinetic}}{E_{PFN}} \times 100 \qquad (18)$$

V. Simulation

In this example, a model of a TC as a linear load will be presented. The TC is modeled by an inductor (L_C) and resistor (R_C), as shown in Fig. 9. The values of them were calculated according to (8) and (11), respectively. By calculating resonance frequency (f_{res}) according to (9), the coil's impedance (Z_C) is obtained according to (12). These calculated values are presented in TABLE II. The TC's total effective inductance and resistance are determined by the inductor and resistor (R_C), which remain constant as the disk accelerates. The desired current pulse profile should have a 100 µs pulse width and 2.4 kA peak magnitude. In the characterization of the PFN to obtain the required current pulse, (1) the charging voltage value, (2) each section's calculated capacitance and inductance values according to (14)-(16), and (3) the required section number should be set as shown in TABLE III. Fig. 10 depicts the equivalent schematic of the computed PFN power supply for TC.

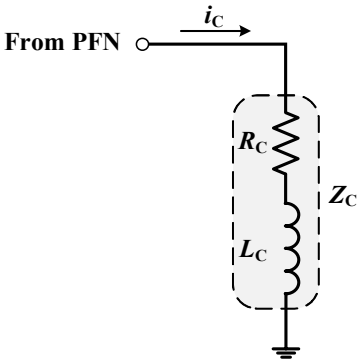

Figure 9. Representation of TC load.

TABLE II. CHARACTERISTICS OF TC

parameter	Data
TC resistance	15.76 mΩ
TC inductance	11.13 µH
TC impedance	71.75 mΩ
Resonance frequency	1 KHz

TABLE III. CHARACTERISTICS OF PFN

parameter	Data
Charge voltage	196 V
Each cell capacitance	17 µF
Each cell inductance	89 nH
Sections number	40

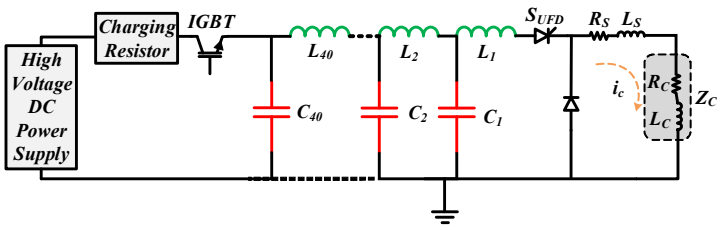

Figure 10. Final simulated Equivalent circuit diagram of a PFN power supply with 40 sections of LC units used for TC (L_1 to L_{40} are the inductors, and C_1 to C_{40} are the capacitors. Z_C is the matched load impedance).

A. Results

To evaluate the suggested structure, the simulation of a PFN-powered TC was conducted in MATLAB SIMULINK.

1) Current

Fig. 11 depicts the PFN output current pulse predicted by the simulation. Fig. 12 shows the differences between the output current pulses with the nominal value of PFN elements and the output current pulse following the capacitor bank. The simulated PFN output current pulse agrees well with the capacitor bank discharge current pulse. Notice that in both of them, the peak current is approximately 2430 A.

2) Displacement and Average Velocity

The black curve represents TC disk displacement supplied by a capacitor bank, while the red curve represents TC disk displacement supplied by a PFN. As demonstrated in the curves, supplying the TC by capacitor bank to reach the required 5 mm travel distance takes 0.48 ms, but supplying the TC in the same condition by PFN takes 0.53 ms. Therefore, according to (6), the average velocity ($\bar{V}$) for a capacitively powered TC is 10.4 m/s, and for a PFN-powered TC is 9.43 m/s. According to (7), the kinetic energy (E_{Kinetic}) for a capacively powered TC is 2.86 J, and for a PFN-powered TC, it is 2.35 J.

3) Electrical-to-kinetic Conversion Efficiency

According to (17), the stored energy in the designed 40 sections PFN (E_{PFN}) with an initial voltage of 196 V is 13.06 J, while the stored energy for the same operation by a capacitor bank (E_{Cap}) according to (3) obtained 62.5 J. According to (13), efficiency for the mentioned capacitor bank power supplied TC ($\eta_{\text{Capacitor}}$) is obtained at 4.5 %, while according to (18), efficiency for the mentioned PFN power supplied TC (η_{PFN}) is obtained at 17.9 %, which shows 13.4 % efficiency improvement.

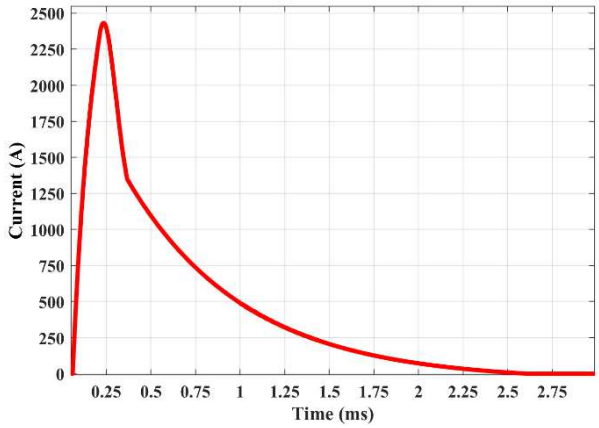

Figure 11. simulated output current pulse of the designed type B PFN injecting into the TC load.

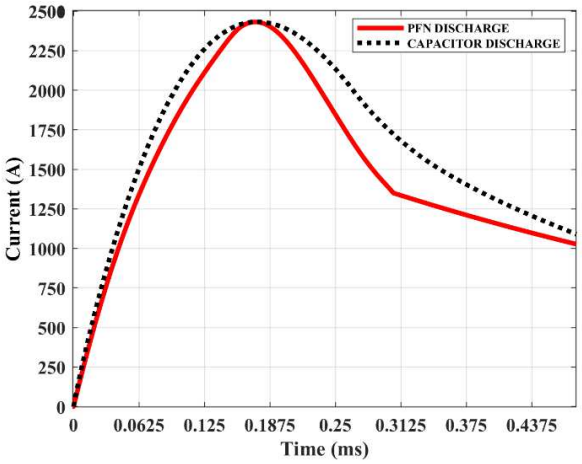

Figure 12. Comparison of the simulated output current pulse of the forty-section PFN and capacitor bank discharge with the same pulse flat top.

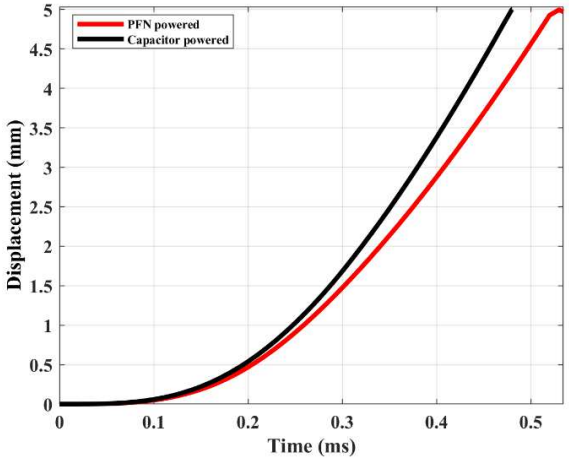

Figure 13. Comparison of the simulated displacement curve of a PFN-supplied and a capacitor bank-supplied TC.

B. Sensitivity Analysis

This section contains a sensitivity analysis that aims to clarify how the various design parameters influence the TC actuator's function. The following analysis concentrates on the impacts of applying pulses with different widths, rise times, and voltages on the improvement of TC efficiency. During the assessment, one parameter is changed from a list of predetermined values, while the others remain constant. The simulation results can be used to establish series of guidelines for TC's mechanical and electrical performance.

1) Average Velocity Sensitivity to Charging Voltage Analysis

Fig. 14 shows the simulation results curve for the average disk velocity ($\bar{V}$) under different charging voltages of the designed 40-section PFN with 17μF capacitors and 89 nH inductors. As shown in Fig. 14, voltage has great effects on the velocity and velocity is increased by increasing the charging voltage.

18th International Conference on Protection & Automation in Power Systems
Shahrood University of Technology
January 9, 2024 - January 10, 2024

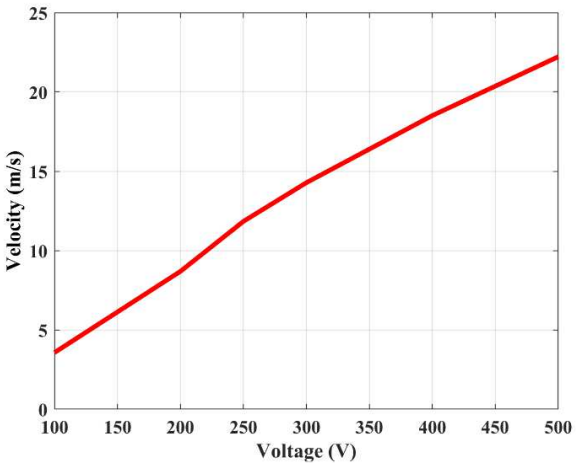

Figure 14. PFN charging voltage effect on average velocity.

2) Efficiency Sensitivity to Charging Voltage Analysis

Fig. 15 shows the simulation results curve for efficiency of the designed 40-section PFN with 17μF capacitors and 89 nH inductors suppling TC actuator under different charging voltages. As shown in Fig. 15, voltage has great effects on efficiency, and efficiency is increased by increasing the charging voltage, but as it can be seen this effect decreases for voltages greater than 300 V, this implies that voltages higher than 300 V are not reasonable.

3) Efficiency Sensitivity to Sections Number and Voltage

Fig. 17, is the summary plot of a PFN-powered TC actuator simulation results obtained from the sensitivity analysis, showing efficiency (Π) for different charging voltages (V) and PFN sections number (n) in a 100 μs current pulse width. It is revealed that the charging voltage (V) between 200-300 V for the PFN and increasing the sections (n) would be the optimal values for the PFN-powered TC-based UFD.

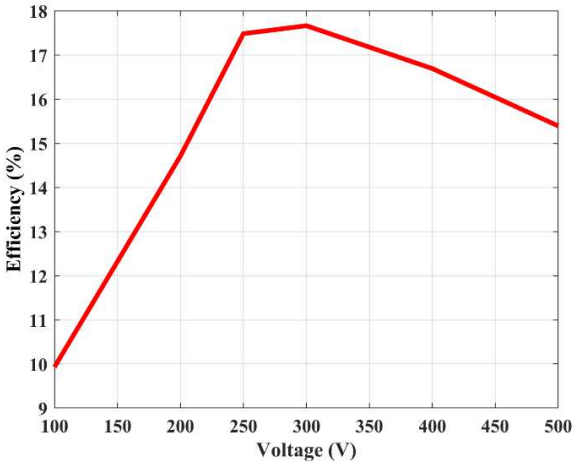

Figure 15. PFN charging voltage effect on efficiency

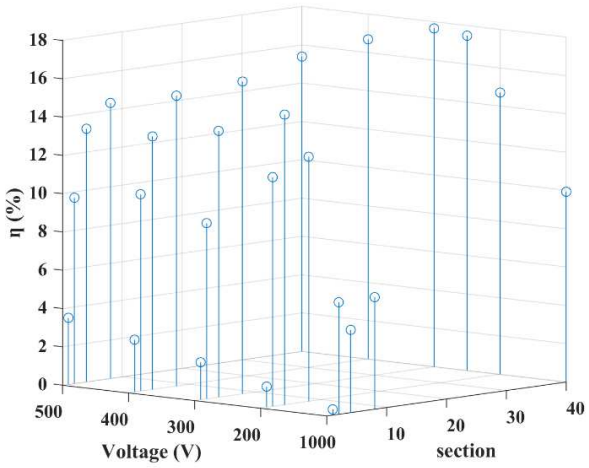

Figure 17. PFN sections number (n) and voltage (V) effect on efficiency (Π) of a 100 μs current pulse width.

VI. Conclusion

The research carried out presented the theoretical results of a PFN-powered TC, and also examined the impact of increased efficiency and component scaling on PFN size for TC actuators. The PFN presented here is charged to 196 V and can deliver a relatively desired current pulse for the nonlinear TC load. This minimizes the need for high-capacitance capacitors, allowing manufacturers to use less expensive capacitors in the drive circuit while meeting practical requirements. The simulated TC used in this research accelerated a 53-gram disk to 9.4 m/s average velocity with a maximum efficiency of 17.6 %, the highest documented for this type of launcher and several times greater than conventional TCs at equivalent mass, size, and velocity. It is concluded that power supplying TC with PFN instead of a capacitor bank is an efficient method and worthy of development.

References

[1] F. Mohammadi et al., "HVDC circuit breakers: A comprehensive review," IEEE Transactions on Power Electronics, vol. 36, no. 12, pp. 13726-13739, 2021.J. Clerk Maxwell, A Treatise on Electricity and Magnetism, 3rd ed., vol. 2. Oxford: Clarendon, 1892, pp.68–73.

[2] S. Wang, C. E. Ugalde-Loo, C. Li, J. Liang, and O. D. Adeuyi, "Bridge-type integrated hybrid DC circuit breakers," IEEE Journal of Emerging and Selected Topics in Power Electronics, vol. 8, no. 2, pp. 1134-1151, 2019.

[3] D. Povh, "Use of HVDC and FACTS," Proceedings of the IEEE, vol. 88, no. 2, pp. 235-245, 2000.R. Nicole, “Title of paper with only first word capitalized,” J. Name Stand. Abbrev., in press.

[4] M. T. Kejani, S. H. Khalkhali, and A. A. Razi-Kazemi, "A New Approach on Condition Assessment of MV Switchgear Based on Thermal Evaluation," in 2023 31st International Conference on Electrical Engineering (ICEE), 2023: IEEE, pp. 904-909. M. Young, The Technical Writer’s Handbook. Mill Valley, CA: University Science, 1989.

[5] I. I. Hussein, S. Essallah, and A. Khedher, "Comparative study of HVDC and HVAC systems in presence of large scale renewable energy sources," in 2020 20th International Conference on Sciences and Techniques of Automatic Control and Computer Engineering (STA), 2020: IEEE, pp. 225-230.

[6] K. Meah and S. Ula, "Comparative evaluation of HVDC and HVAC transmission systems," in 2007 IEEE Power Engineering Society General Meeting, 2007: IEEE, pp. 1-5.

[7] T. Halder, "Comparative study of HVDC and HVAC for a bulk power transmission," in 2013 International Conference on Power, Energy and Control (ICPEC), 2013: IEEE, pp. 139-144.

[8] M. T. Kejani, S. H. Aleyasin, A. Safaeinasab, and K. Abbaszadeh, "A new non-isolated single switch high step-up DC/DC converter based on inductor cells," in 2021 12th Power Electronics, Drive Systems, and Technologies Conference (PEDSTC), 2021: IEEE, pp. 1-5.

[9] Z. Yuan et al., "Research on ultra-fast vacuum mechanical switch driven by repulsive force actuator," Review of Scientific Instruments, vol. 87, no. 12, p. 125103, 2016.

[10] D. S. Vilchis - Rodriguez, R. Shuttleworth, A. C. Smith, and M. Barnes, "Comparison of damping techniques for the soft - stop of ultra - fast linear actuators for HVDC breaker applications," The Journal of Engineering, vol. 2019, no. 17, pp. 4466-4470, 2019.

[11] M. Al-Dweikat, J. Cui, S. Sun, M. Yang, G. Zhang, and Y. Geng, "A review on Thomson coil actuators in fast mechanical switching," in Actuators, 2022, vol. 11, no. 6: MDPI, p. 154.

[12] B. Yin, X. Pei, X. Zeng, and F. Eastham, "A comparison between moving magnet and moving coil actuators for vacuum interrupters," in IECON 2019-45th Annual Conference of the IEEE Industrial

[13] G. Li, J. Liang, S. Balasubramaniam, T. Joseph, C. E. Ugalde-Loo, and K. F. Jose, "Frontiers of DC circuit breakers in HVDC and MVDC systems," in 2017 IEEE conference on energy internet and energy system integration (EI2), 2017: IEEE, pp. 1-6.

[14] P. Heidary, S. H. Khalkhali, M. T. Kejani, and A. A. Razi-Kazemi, "Design and Simulation of an Electromagnetic Actuator for a Linear Ultra-fast Disconnector (UFD) with Mechanical Stress Consideration," in 2023 27th International Electrical Power Distribution Networks Conference (EPDC), 2023: IEEE, pp. 136-141.

[15] S. H. Khalkhali, M. T. Kejani, and A. A. Razi-Kazemi, "Design of an Electromagnetic Actuator for a 2MW DC Circuit Breaker with a Fast Mechanical Switch Installed in the Railway Distribution Grid," in 2023 27th International Electrical Power Distribution Networks Conference (EPDC), 2023: IEEE, pp. 1-5.

[16] S. H. Khalkhali and A. A. Razi-Kazemi, "Design of a Combined Mechanical and Electrical Damper to Reduce Contact Speed at the Moment of Collision at the Endpoint," in 2022 13th Power Electronics, Drive Systems, and Technologies Conference (PEDSTC), 2022: IEEE, pp. 328-333.

[17] M. Zaja, A. A. Razi - Kazemi, and D. Jovcic, "Detailed electro - dynamic model of an ultra - fast disconnector including the failure mode," High Voltage, vol. 5, no. 5, pp. 549-555, 2020.

[18] M. Hedayati and D. Jovcic, "Low voltage prototype design, fabrication and testing of ultra-fast disconnector (UFD) for hybrid DC CB," in Proc. CIGRE B4 Colloq., 2017, pp. 1-6.

[19] D. Jovcic, M. Zaja, and M. H. Hedayati, "Bidirectional hybrid HVDC CB with a single HV valve," IEEE Transactions on Power Delivery, vol. 35, no. 1, pp. 269-277, 2019.

[20] M. Callavik, A. Blomberg, J. Häfner, and B. Jacobson, "The hybrid HVDC breaker," ABB Grid Systems Technical Paper, vol. 361, pp. 143-152, 2012.

[21] A. Hassanpoor and J. Häfner, "Abb power grids hybrid hvdc breaker full-scale test: A breakthrough towards hvdc grid realization," in ABB, 2020.

[22] C. Peng, I. Husain, A. Q. Huang, B. Lequesne, and R. Briggs, "A fast mechanical switch for medium-voltage hybrid DC and AC circuit breakers," IEEE Transactions on Industry Applications, vol. 52, no. 4, pp. 2911-2918, 2016.

[23] Y. Zhou, Y. Huang, W. Wen, J. Lu, T. Cheng, and S. Gao, "Research on a novel drive unit of fast mechanical switch with modular double capacitors," The Journal of Engineering, vol. 2019, no. 17, pp. 4345-4348, 2019.

[24] H. A. Wheeler, "Simple inductance formulas for radio coils," Proceedings of the institute of Radio Engineers, vol. 16, no. 10, pp. 1398-1400, 1928.

[25] A. Kadivar, "Electromagnetic Actuators for Ultra-fast Air Switches to Increase Arc Voltage by Increasing Contact Speed," in 2019 International Power System Conference (PSC), 2019: IEEE, pp. 256-262.

[26] D. Vilchis-Rodriguez, R. Shuttleworth, and M. Barnes, "Finite element analysis and efficiency improvement of the Thomson coil actuator," in 8th IET International Conference on Power Electronics, Machines and Drives (PEMD 2016), 2016: IET, pp. 1-6.

[27] M. Barnes, D. S. Vilchis-Rodriguez, X. Pei, R. Shuttleworth, O. Cwikowski, and A. C. Smith, "HVDC circuit breakers–A review," IEEE Access, vol. 8, pp. 211829-211848, 2020.

[28] D. S. Vilchis - Rodriguez, R. Shuttleworth, A. C. Smith, and M. Barnes, "Performance of high - power thomson coil actuator excited by a current pulse train," The Journal of Engineering, vol. 2019, no. 17, pp. 3937-3941, 2019.

[29] S. Mohsenzade, M. Zarghany, M. Aghaei, and S. Kaboli, "A high-voltage pulse generator with continuously variable pulsewidth based on a modified PFN," IEEE Transactions on Plasma Science, vol. 45, no. 5, pp. 849-858, 2017.

[30] G.-H. Rim, E. P. Pavlov, H.-S. Lee, J. S. Kim, and Y.-W. Choi, "Pulse forming lines for square pulse generators," IEEE transactions on plasma science, vol. 31, no. 2, pp. 196-200, 2003.

[31] A. Musolino, M. Raugi, and B. Tellini, "Pulse forming network optimal design for the power supply of EML launchers," IEEE Transactions on Magnetics, vol. 33, no. 1, pp. 480-483, 1997.